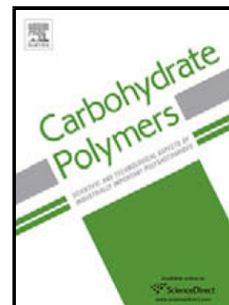


Accepted Manuscript

Title: Enhanced delivery of doxorubicin to the liver through self-assembled nanoparticles formed via conjugation of glycyrrhetic acid to the hydroxyl group of hyaluronic acid

Authors: Xiaodan Wang, Xiangqin Gu, Huimin Wang, Jingyu Yang, Shirui Mao



PII: S0144-8617(18)30438-7
DOI: <https://doi.org/10.1016/j.carbpol.2018.04.052>
Reference: CARP 13506

To appear in:

Received date: 5-12-2017
Revised date: 13-3-2018
Accepted date: 11-4-2018

Please cite this article as: Wang, Xiaodan., Gu, Xiangqin., Wang, Huimin., Yang, Jingyu., & Mao, Shirui., Enhanced delivery of doxorubicin to the liver through self-assembled nanoparticles formed via conjugation of glycyrrhetic acid to the hydroxyl group of hyaluronic acid. *Carbohydrate Polymers* <https://doi.org/10.1016/j.carbpol.2018.04.052>

This is a PDF file of an unedited manuscript that has been accepted for publication. As a service to our customers we are providing this early version of the manuscript. The manuscript will undergo copyediting, typesetting, and review of the resulting proof before it is published in its final form. Please note that during the production process errors may be discovered which could affect the content, and all legal disclaimers that apply to the journal pertain.

Enhanced delivery of doxorubicin to the liver through self-assembled nanoparticles formed via conjugation of glycyrrhetic acid to the hydroxyl group of hyaluronic acid

Xiaodan Wang¹, Xiangqin Gu¹, Huimin Wang¹, Jingyu Yang², Shirui Mao^{1,*}

¹School of Pharmacy, Shenyang Pharmaceutical University, Shenyang 110016, China

²Department of Pharmacology, Shenyang Pharmaceutical University, Shenyang, 110016, China

* To whom correspondence should be addressed.

School of Pharmacy

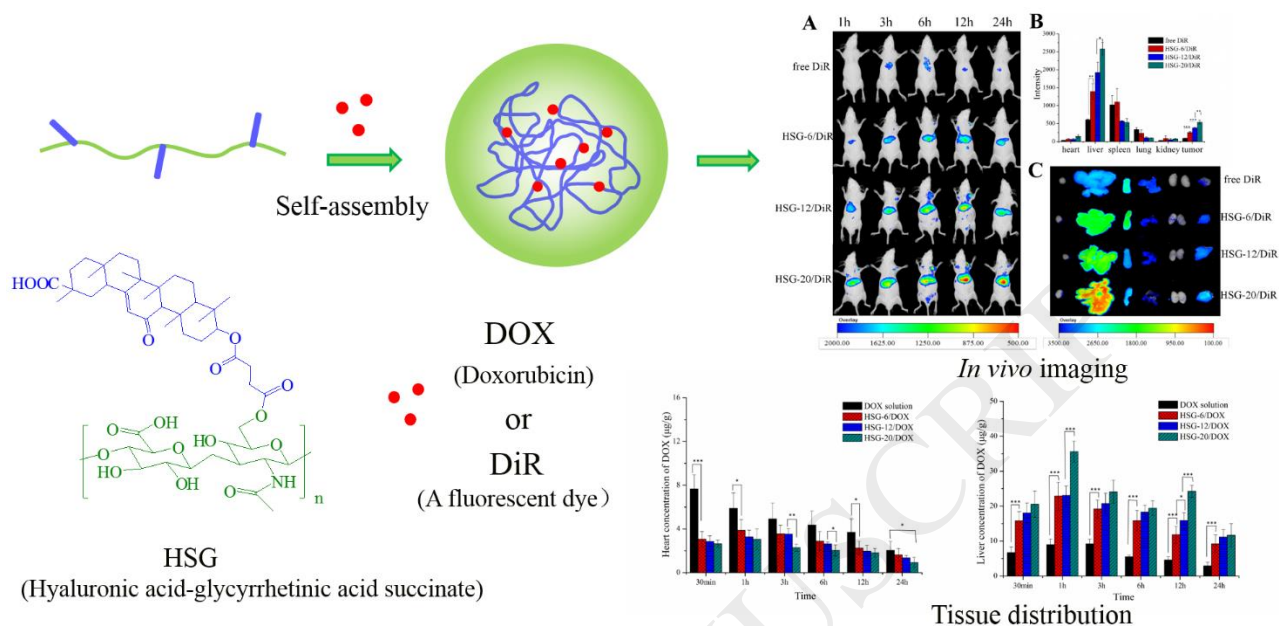
Shenyang Pharmaceutical University

Shenyang, China

Tel and Fax: +86-24-43520523

E-mail: maoshirui@syphu.edu.cn; maoshirui@vip.sina.com

Graphic abstract



Highlights

- Enhanced delivery of doxorubicin to the liver through self-assembled nanoparticles formed via conjugation of glycyrrhetic acid to the hydroxyl group of hyaluronic acid was demonstrated for better therapy of hepatocytes.
- Doxorubicin-loaded nanoparticles presented higher liver and tumor targeting efficiency, and the higher glycyrrhetic acid graft ratio on hyaluronic acid, the better liver and tumor targeting property.
- The binding site of glycyrrhetic acid on hyaluronic acid has significant influence on the liver and tumor targeting efficiency.

Abstract

Liver-targeted nanoparticles is highly desired for better therapy of liver cancer. In this study, enhanced delivery of doxorubicin (DOX) to the liver cells through self-assembled nanoparticles formed via conjugation of glycyrrhetic acid (GA) to the hydroxyl group of hyaluronic acid (HA) was investigated. The DOX loaded hyaluronic acid-glycyrrhetic acid succinate (HSG) conjugates based nanoparticles (HSG/DOX nanoparticles) were sub-spherical in shape with particle size in the range of 180-280 nm, the drug loading was drug-to-carrier ratio and GA graft ratio dependent. *In vitro* release study suggested that the release of DOX from HSG nanoparticles was sustained and the release rate was pH and GA graft ratio dependent. MTT assay indicated the HSG/DOX nanoparticles presented a GA-dependent cytotoxicity to HepG2 cells. Pharmacokinetics study demonstrated the HSG/DOX nanoparticles could prolong blood circulation time of DOX and had a higher AUC value than that of DOX solution. Furthermore, tissue distribution study revealed the HSG/DOX nanoparticles significantly increased the accumulation of DOX in the liver and meanwhile decreased the cardiotoxicity and nephrotoxicity of DOX. Moreover, the liver targeting enhancing capacity was HSG conjugate structure dependent. The accumulation of HSG-20/DOX, HSG-12/DOX, and HSG-6/DOX nanoparticles in the liver was 4.0-, 3.1-, and 2.6-fold higher than that of DOX solution. *In vivo* imaging analysis further demonstrated HSG nanoparticles not only had better liver targeting effect, but also presented superior tumor targeting efficiency, and the tumor targeting capacity was also GA-dependent. These results indicated that HSG conjugates prepared via modifying the hydroxyl groups of HA have promising potential as a liver-targeting nanocarrier for the delivery of hydrophobic anti-tumor drugs.

Keywords: Hyaluronic acid; Glycyrrhetic acid; Nanoparticles; Doxorubicin; Liver-targeting

1. Introduction

Treatment of liver cancer has become a major problem because of its high morbidity and high mortality (Torre, Bray, Siegel, Ferlay, Lortet-Tieulent & Jemal, 2015). In recent years, significant efforts have been exerted towards the design and construction of liver-targeted nanoparticles for better therapy of hepatocytes (Jiang et al., 2009; Krishna, Mandraju, Kishore & Kondapi, 2009; Liu et al., 2011). However, the introduction of liver targeting moieties often complicate the preparation of nanoparticles. In order to simplify the system, hydrophilic or hydrophobic materials with active targeting have generated considerable interests as the carrier for nanoparticle drug delivery system design (Arpicco, Milla, Stella & Dosio, 2014; Schante, Zuber, Herlin & Vandamme, 2011; Tian, Wang, Wang, Zhang, Wang & Yuan, 2012).

Hyaluronic acid (HA) is a promising hydrophilic material in the area of nanoparticle system design (Choi et al., 2010; Choi, Saravanakumar, Park & Park, 2012), because it can specifically bind to the CD44 (Arpicco, Milla, Stella & Dosio, 2014; Tripodo, Trapani, Torre, Giammona, Trapani & Mandracchia, 2015), RAHMM (Schiffelers et al., 2004) and LYVE-1 receptors (Bhang et al., 2009), which are over-expressed in various kinds of malignant cells including the hepatoma cell line. Son et al. prepared hyaluronic acid-poly(D,L-lactide-co-glycolide) polymeric micelles and confirmed that the HA micelles could enter HepG2 cells via CD44 receptor-mediated endocytosis, and thus delivered DOX into HepG2 cells, leading to strong cytotoxicity (Son et al., 2014).

Glycyrrhetic acid (GA), one of the main bioactive compounds of licorice, has been widely used in pharmaceutical field for the treatment of many pathologies (Lu, Li & Wang, 2008). Due to its remarkable physicochemical characteristics, such as its hydrophobicity (Wang, Tian, Wang, Zhang, Wang & Yuan, 2012) and targeting properties (Tian et al., 2010), GA has been applied in nano-drug delivery systems especially for chemotherapy of hepatocyte (Cai, Xu, Chan, Fang, He & Chen, 2016; Guo et al., 2013). Due to the abundant GA receptors on hepatocyte membranes,

nanoparticles containing GA presented higher accumulation in the liver, and thereby have better therapy of hepatocytes (Tian, Wang, Wang, Zhang, Wang & Yuan, 2012; Tian et al., 2010). Moreover, Tian et al. found that GA-modified micelles could discriminate the normal liver cells and the liver cancer cells, and there was 2.18-fold improvement in uptake by HepG2 cells than that by normal liver cells (Tian, Wang, Wang, Zhang, Wang & Yuan, 2012). And the ability of GA-modified micelles to selectively kill liver malignant cells has been demonstrated by Zhang et al (Zhang et al., 2012), which resulted in higher therapeutic efficacy with improved safety.

Therefore, based on the active liver targeting capacity originated from both HA and GA, it is assumed that HA-GA conjugation as drug carrier may lead to synergistic liver targeting effect (Han et al., 2016; Mezghrani et al., 2015; Zhang, Yao, Zhou, Wang & Zhang, 2013). And the two reactive groups (the carboxyl and hydroxyl group) in the backbone of HA (Choi et al., 2010; Schante, Zuber, Herlin & Vandamme, 2011), make it flexible to modify GA molecule as required (Han et al., 2016; Mezghrani et al., 2015; Zhang, Yao, Zhou, Wang & Zhang, 2013). Our previous studies (Wang, Gu, Wang, Sun, Wu & Mao, 2017) demonstrated that hyaluronic acid-glycyrrhetic acid succinate (HSG) synthesized by modifying hydroxyl groups of HA could provide superior liver targeting efficiency compared to carboxyl group modification. Thus, it is reasonable to assume that by using this conjugate as the drug nanocarrier, which can be prepared by self-assemble using HA as the hydrophilic part and GA as the hydrophobic part, better liver targeting efficiency can be achieved with decreased side effect.

In this study, doxorubicin (DOX) was chosen as a model drug because it has been extensively used in clinic for liver cancer therapy (Li & Wallace, 2008) and the DOX nano-delivery systems have been widely concerned (Kataoka. et al., 2000; Matsumura & Kataoka, 2009; Shuai, Ai, Nasongkla, Kim & Gao, 2004). DOX-loaded HSG nanoparticles were prepared and their physicochemical properties were characterized including particle size, morphology, drug loading, and *in vitro* release performance. The cytotoxicity, pharmacokinetics and the liver and tumor targeting ability of DOX-loaded HSG nanoparticles were also investigated. Moreover,

considering that GA presented two functions, as the hydrophobic group and meanwhile as the liver targeting ligand, its amount might greatly affect the physicochemical properties and fate of nanoparticles, thus, influence of GA graft ratio on the properties of HSG nanoparticles was further elucidated.

2. Materials and methods

2.1. Materials

Hyaluronic acid (HA, 100 kDa) was obtained by oxidative depolymerization (Hokputsa, Jumel, Alexander & Harding, 2003) of HA (200 kDa) supplied by Xian Rongsheng Biotechnology Co. Ltd. (Shanxi, China). Glycyrrhetic acid (GA) was purchased from Nanjing Zelang Medicine Technology Co. Ltd. (Jiangsu, China). Succinic anhydride was from Tianjin Bodi Chemical Holding Co. Ltd. (Tianjin, China). N, N-dicyclohexyl carbodiimide (DCC) and 4-dimethylaminopyridine (DMAP) were from Shanghai Sinopharm Chemical Reagent Co. Ltd. (Shanghai, China). Doxorubicin hydrochloride (DOX·HCl) was purchased from Beijing Huafeng Lianbo Technology Co. Ltd. (Beijing, China). All other chemicals were of analytical grade and were used without further purification.

2.2. Synthesis and characterization of hyaluronic acid-glycyrrhetic acid succinate conjugates

Hyaluronic acid-glycyrrhetic acid succinate (HSG) conjugates were synthesized via two steps as reported previously (Wang, Gu, Wang, Sun, Wu & Mao, 2017). Firstly, GA (5.0 mmol), succinic anhydride (20.0 mmol) and DMAP (5.0 mmol) in 60 mL of DCM was refluxed at 40°C for 12 h, then the DCM was removed by evaporation. The precipitate was washed with water, then filtered and dried. Pure 3-O-hemi-succinate GA (suc-GA) was obtained by recrystallization in ethanol. Secondly, suc-GA was reacted with DCC and DMAP in 20 mL of DMF at 0°C for 3 h and the molar ratio of DCC:DMAP:suc-GA was 4:1.33:1. Briefly, HA (200 mg) in 10 mL of formamide was reacted with different amounts of activated suc-GA at 40°C for 36 h. The solution was dialyzed against DMSO for 2 days and distilled water for 3 days using a dialysis membrane (MWCO: 8,000-14,000). The dialyzed solution was

lyophilized to obtain the white, sponge-like HSG conjugates.

The structure of HSG was confirmed by ¹H-NMR (AV-600, Bruker, Germany) and FT-IR (IFS-55, Bruker, Switzerland). The degree of substitution (DS), defined as the number of GA groups per 100 disaccharide units of HA, was estimated by UV-Vis spectrophotometer (UV-2000, Unico, Shanghai, China) at 250 nm (Zhang, Yao, Zhou, Wang & Zhang, 2013). The DS was calculated with the following equation:

$$DS(\%) = \frac{\text{Concentration of GA} / \text{Molecular mass of GA}}{(\text{Concentration of HSG} - \text{Concentration of GA}) / \text{Molecular mass of unit of HA}} \times 100$$

2.3. Preparation of DOX-loaded HSG nanoparticles

The DOX-loaded HSG nanoparticles were prepared by dialysis method (Wu, Liu, Wang & Huang, 2012). Briefly, 20 mg of lyophilized HSG was dissolved in 2 mL of formamide with stirring for 3 h at room temperature. Different amounts of DOX·HCl were stirred in 1 mL of dimethylformamide overnight in the presence of triethylamine (3 times molar quantity of DOX·HCl). The above polymer and DOX solution were mixed and stirred for 24 h, followed by dialysis against distilled water for 24 h using a dialysis membrane (MWCO: 8,000-14,000). The outer solution was exchanged at 3-h intervals. Subsequently, the dialyzed solution was filtered through a 0.8 μm millipore membrane and then lyophilized.

2.4. Characterization of DOX-loaded HSG nanoparticles

2.4.1. Determination of the drug loading and encapsulation yields

Approximately 2mg of lyophilized DOX-loaded HSG nanoparticles were dissolved in 2 mL formamide, and the amount of DOX in nanoparticles was determined by UV-Vis spectrophotometer (UV-2000, Unico, Shanghai, China) at 480 nm (Wu, Liu, Wang & Huang, 2012). The drug loading (DL) and encapsulation yields (EY) were calculated as follow:

$$DL(\%) = \frac{\text{Weight of DOX in nanoparticles}}{\text{Weight of HSG/DOX nanoparticles}} \times 100$$
$$EY(\%) = \frac{\text{Weight of DOX in nanoparticles}}{\text{Weight of DOX used for nanoparticles preparation}} \times 100$$

2.4.2. Particle size and zeta potential

The particle size and the zeta potential of the HSG/DOX nanoparticles or the blank nanoparticles were measured by dynamic light scattering and laser doppler anemometry, respectively, using the Zetasizer (NANOZS90, Malvern Instruments, UK) at 25°C.

2.4.3. Morphological observation

The morphology of HSG/DOX nanoparticles was observed using transmission electron microscopy (TEM, JEM-2100, Japan) with an accelerating voltage of 200 kV. A drop of the sample solution was placed onto a 300-mesh copper grid with carbon. And then the sample was taped with a filter paper to remove surface water and air-dried. The sample was negatively stained with 2% phosphotungstic acid before observation.

2.4.4. Differential scanning calorimetry analysis

The existing state of DOX in nanoparticles was determined by differential scanning calorimetry (DSC). Analysis of DOX, blank HSG nanoparticles, HSG/DOX nanoparticles, physical mixture of DOX and blank HSG nanoparticles was carried out using DSC equipment (Zürich, Switzerland), respectively. The temperature ranged from 30°C to 300°C and the heating rate was 10°C/min.

2.5. *In vitro* release

The *in vitro* release behavior of DOX from the nanoparticles was evaluated in phosphate-buffered saline (PBS) solutions of various pH (pH 5.5, 6.5 and 7.4), using a dialysis method (MCWO: 8,000-14,000) (Wu, Liu, Wang & Huang, 2012). Briefly, 2 mL of HSG/DOX nanoparticles was transferred in dialysis bags and then dialyzed against 50 mL of PBS at 37°C in an air-bath shaker under stirring at 100 rpm. The system was protected from light. At predetermined time intervals (0, 1, 2, 4, 6, 8, 12, 24, 36, 48 h), 2 mL of the medium were taken out and replaced with an equal volume of fresh medium. The amount of released DOX was determined by UV-Vis

spectrophotometer (UV-2000, Unico, Shanghai, China) at 480 nm.

2.6. *In vitro* cytotoxicity assay

The cytotoxicity of the HSG/DOX nanoparticles and DOX solution against HepG2 cells were determined using the MTT (3-(4,5-Dimethylthiazol)-2-yl)-2,5-diphenyltetrazolium bromide) assay (Wang et al., 2014). Briefly, HepG2 cells (5.0×10^3) were seeded in each well of a 96-well plate and were incubated for 24 h at 37°C to allow cell attachment. Then, the cells were incubated with the HSG/DOX nanoparticles or DOX solution (final concentrations of DOX were 0.03, 0.1, 0.3, 1 and 3 µg/mL) for 24 h. Following incubation, 20 µL of MTT solution (5.0 mg/mL) was added, and the cells were further incubated for another 4 h. Thereafter, the MTT medium was removed from each well, and 150 µL of DMSO was added to dissolve the formazan crystals. Absorbance was measured at 570 nm with a multimode microplate reader (SpectraMax M3, Molecular Devices, US). The untreated cells were taken as control. The relative cell viability (%) was calculated as (absorbance of test group/ absorbance of control group) \times 100.

2.7. Pharmacokinetic study in rats

Sprague–Dawley (SD) rats were used to evaluate the pharmacokinetics of the HSG/DOX nanoparticle. All animal studies were approved by the University Ethics Committee and were carried out in accordance with the Principle of Laboratory Animal Care. Twenty SD rats (male, 200 ± 20 g) were randomly divided into four groups. HSG/DOX nanoparticles and DOX solution were intravenously administered via a tail vein at a single dose of 5 mg DOX/kg. Blood samples (about 500 µL) were collected from retro-orbital plexus into heparinized tubes at 0.083, 0.25, 0.5, 1, 2, 3, 4, 6, 8, 10, 12, and 24 h and then centrifuged at 10,000 rpm for 10 min. The plasma samples were stored at -20°C until analysis.

Extraction of doxorubicin from the plasma was carried out as described in the previous report with slight modifications (Guo et al., 2014). Briefly, plasma sample (200 µL) was added to 2.8 mL of extraction solvent (0.3 M HCl/EtOH=3/7, v/v) and

the mixture was vortex mixed for 5 min. After centrifugation at 10,000 rpm for 10 min, the supernatant was transferred and used for fluorescence measurement by a multimode microplate reader (SpectraMax M3, Molecular Devices, US) at excitation/emission wavelength of 500/588 nm.

2.8. Tissues Distribution Study

Kun Ming (KM) mice were used to assess the effect of different formulations on tissue distribution of DOX. One hundred and twenty KM mice (male, 20 ± 2 g) were randomly divided into four groups. HSG/DOX nanoparticles and DOX solution were intravenously administered via a tail vein at a single dose of 5 mg DOX/kg. At different time points (0.5, 1, 3, 6, 12, and 24 h) post injection, the mice were sacrificed and the major organs (heart, liver, spleen, lung, and kidney) were collected. All the tissues samples were stored at -20°C until analysis.

The isolated tissue samples were weighed accurately and homogenized with 0.9%NaCl solution (tissue samples/0.9%NaCl=1/2, g/mL). Thereafter, the tissue homogenates were processed using the same method for plasma samples as described above and drug content in each tissue was determined.

2.9 Evaluation of tumor targeting effect by in vivo imaging

For *in vivo* imaging analysis, near infrared fluorescent dye, DiR was incorporated into HSG nanoparticles as reported previously (Wang, Gu, Wang, Sun, Wu & Mao, 2017). The amount of DiR in HSG-6, HSG-12, and HSG-20 nanoparticles was calculated to be 0.87%, 0.95%, and 1.03%, respectively, and the particle sizes were 257.6, 231.1, and 168.9 nm, respectively ($n=3$). There was no significant difference between the size of HSG/DiR nanoparticles and HSG/DOX nanoparticles ($p > 0.05$).

To evaluate the tumor targeting ability of HSG nanoparticles, BALB/c nude mice (six weeks old, 20-25 g) were used to generate HeGp2 tumor-xenografted mouse model (Huo et al., 2012). Twelve tumor-bearing mice were randomly divided into four groups. HSG/DiR nanoparticles and DiR solution were injected into the

tumor-bearing mice via a tail vein at a dose of 100 μg DiR/kg, respectively. The near infrared fluorescent imaging were performed at 1, 3, 6, 12, and 24 h after injection using an *in vivo* Imaging System (FX, Kodak, USA), and the excitation and emission wavelengths were 720 nm and 790 nm, respectively. After living imaging, the tumor-bearing mice were sacrificed. The major organs including liver, lung, spleen, kidney, heart, as well as the tumor, were dissected from the mice, and the fluorescence intensity was determined again with the same system as described above.

2.10. Statistical analysis

All data were expressed as means \pm SD from at least three different experiments. The pharmacokinetic parameters were calculated using DAS (Drug and Statistics) 2.0 software. A two-tail paired Student's t-test was used to compare the difference. Probability value $p < 0.05$ was considered statistically significant.

3. Results and discussion

3.1. Synthesis and characterization of HSG conjugates

HSG conjugates were synthesized by modifying the hydroxyl group with the help of succinic anhydride (Supplementary Materials Fig. S1) and the conjugates were coded as HSG-X, where X represents the GA graft ratio. The successful synthesis of HSG was confirmed by $^1\text{H-NMR}$ and FT-IR (Supplementary Materials Fig. S2, Fig.S3). A new multiplet at 2.65 ppm observed in the spectrum of suc-GA can be attributed to the two adjacent methylene groups of the succinyl moiety, suggesting that succinyl group was attached to GA successfully. In comparison with HA, the characteristic peaks of GA at 0.8-1.7 ppm, corresponding to the methyl and methylene groups, appeared in the spectrum of HSG-20, indicating GA was successfully conjugated to the backbone of HA. Compared with HA, in the spectrum of HSG-20, a new absorption peak emerged at 1729 cm^{-1} , which can be attributed to the newly formed ester carbonyl group. Simultaneously, the intensity at $2930\sim 2850\text{ cm}^{-1}$ was enhanced sharply in the spectrum of HSG-20, which can be attributed to the carbon-to-hydrogen stretching vibrations from the large number of methyl and

methylene groups of GA moiety in HSG-20, further suggesting that GA has been attached to HA backbone successfully.

3.2. Influence of drug-to-carrier ratio on the characteristics of DOX-loaded HSG nanoparticles

DOX-loaded HSG nanoparticles were prepared via self-assembly and DOX was loaded into the nanoparticles based on its hydrophobic and electronic interaction with the HSG conjugate. First of all, taking HSG-12/DOX nanoparticles as an example, influence of drug-to-carrier ratio on the characteristics of DOX-loaded HSG nanoparticles was investigated. As shown in Table 1, drug-to-carrier ratio could significantly affect properties of the nanoparticles. As the drug-to-carrier ratio increased from 5% to 20%, the drug loading increased from 5.01% to 12.48%, however, the encapsulation yields decreased from 95.47% to 65.04%. When further increasing drug-to-carrier ratio from 20% to 30%, the drug loading only increased slightly (from 12.48% to 13.24%), but the encapsulation yields decreased significantly (from 65.04% to 45.01%). As to the influence on particle size, when drug-to-carrier ratio was 5%, the particle size was smaller than the blank nanoparticles ($p < 0.05$). The result suggested that hydrophobic DOX might make a tightly packed hydrophobic core at low drug loading (Lao, Zhang, Xu & Jiang, 2010). But when drug-to-carrier ratio was increased up to 10%, the addition of higher amount of drugs could enlarge the inner core volume, compromising the impact of hydrophobic interaction, thus no significant change in particle size was found ($p > 0.05$). Further increasing drug-to-carrier ratio to 20% and 30% caused significant increase in particle size ($p < 0.05$), this can probably be explained by the fact that at specific GA graft ratio, the hydrophobic interaction between drug and GA will be saturated at higher drug loading, thus the additional drug incorporation will lead to core volume increase (Xiangyang et al., 2007), therefore increased particle size. Moreover, it was noticed that compared with the blank nanoparticles, zeta potentials of all the HSG/DOX nanoparticles decreased significantly ($p < 0.05$), indicating the presence of electrostatic interaction between the drug and nanoparticles, but the

influence of drug loading amount on zeta potential was insignificant ($p>0.05$). Therefore, it is reasonable to conclude that hydrophobic interactions are the major binding force to load DOX into HSG/DOX nanoparticles. Taking both drug loading and encapsulation yield into account, unless otherwise specified, HSG/DOX nanoparticles prepared at drug-to-carrier ratio 20% were used in the following studies.

3.3. Influence of GA graft ratio on the characteristics of DOX-loaded HSG nanoparticles

By keeping drug-to-carrier ratio 20%, influence of GA graft ratio on the characteristics of DOX-loaded HSG nanoparticles was investigated. As shown in Table 1, by increasing GA graft ratio from 6% to 20%, the drug loading and encapsulation yields increased significantly ($p<0.05$), which could be attributed to the stronger hydrophobic interactions, therefore increased DOX loading. Meanwhile, particle size of HSG/DOX nanoparticles decreased with the increase of GA graft ratio and it decreased from 281.7 nm at GA ratio 6% to 184.8nm at GA ratio 20%, with sharp particle size distribution (Fig. 1A). This can probably be explained by the enhanced hydrophobic interaction between GA groups and DOX, making the inner core more compacted, therefore smaller particle size.

Table 1. Effect of drug-to-carrier ratio and GA graft ratio on the properties of HSG/DOX nanoparticles (n=3).

Sample	Drug/carrier (w/w, %)	Size (nm)	PDI	Zeta (mV)	DL (wt%)	EY (wt%)
HSG-6/DOX	20	281.7±6.7	0.035±0.028	-27.2±1.0	9.66±0.44	50.12±2.39
HSG-12/DOX	0	213.4±3.5	0.098±0.048	-34.9±0.6	-	-
	5	204.4±4.2	0.109±0.031	-30.4±1.6	5.01±0.19	95.47±3.69
	10	212.4±2.3	0.154±0.016	-29.5±1.9	7.62±0.32	80.25±3.41
	20	235.9±4.1	0.110±0.042	-28.2±0.8	12.48±0.74	65.04±3.82
	30	248.6±3.8	0.066±0.048	-26.4±1.1	13.24±0.61	45.01±2.06
HSG-20/DOX	20	184.8±3.3	0.188±0.042	-31.3±0.6	13.94±0.65	72.90±3.41

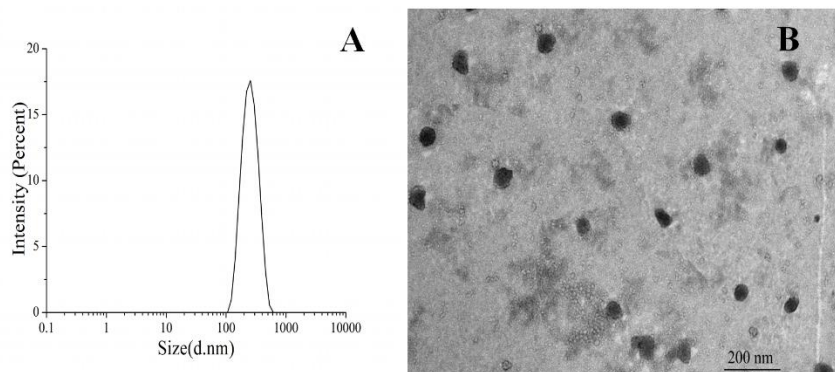


Fig. 1. Particle size distribution measured by dynamic light scattering (DLS) (A) and TEM image (B) of the HSG-12/DOX nanoparticles prepared at drug-to-carrier ratio of 20%.

Morphology of HSG / DOX nanoparticles was visualized by TEM. Fig. 1B exemplifies that HSG-12/DOX nanoparticles were sub-spherical in shape and the observed particle size was approximately 50 nm, which was smaller than the hydrodynamic diameter obtained from DLS measurement (Table 1). This discrepancy might be due to the shrinkage of hydrophilic shell of nanoparticles during the drying process of TEM samples preparation (Han, Han, Lee, Kang, Kim & Park, 2011).

To confirm the existing state of DOX in the HSG nanoparticles, DSC analyses were performed for DOX, blank HSG nanoparticles, HSG-12/DOX nanoparticles, corresponding physical mixture of DOX and blank HSG nanoparticles, respectively, and the thermograms are presented in Fig. 2. Obviously, the DSC thermogram of DOX exhibit an endothermic peak at 205°C. The characteristic peaks of DOX did not occur in the thermogram of HSG-12/DOX nanoparticles, but appeared in the physical mixture of DOX and blank HSG nanoparticles, indicating that DOX existed in amorphous state in the HSG nanoparticles (Huo et al., 2012).

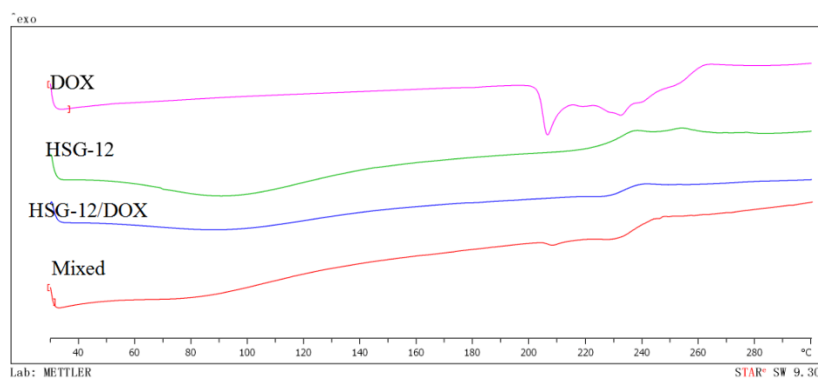


Fig. 2. DSC spectra of DOX, HSG-12 blank nanoparticles, physical mixture of DOX and blank HSG nanoparticles, and HSG-12/DOX nanoparticles.

3.4. Release behavior of doxorubicin from the nanoparticles

First of all, influence of system pH on the *in vitro* release of DOX from HSG nanoparticles was investigated. As shown in Fig. 3, HSG/DOX nanoparticles exhibited a pH-dependent DOX release pattern, which can be explained by the pH-dependent solubility of DOX (Guo et al., 2014). For instance, HSG-20/DOX released nearly 51% of DOX in PBS at pH 5.5 after 48 h, which was significantly higher than that at pH 6.5 (35%) ($p < 0.05$) and at pH 7.4 (29%) ($p < 0.01$). This pH-dependent release behavior is advantages for liver targeting drug delivery system design while it can result in a sustained release of DOX in the bloodstream (pH 7.4) to prolong drug circulation time and lead to a faster release into the extracellular matrix of tumor (pH 6.5) or inside the endosome/lysosome of tumor cells (pH 5.5) to achieve better tumor-targeted drug delivery (Egusquiaguirre, Igartua, Hernandez & Pedraz, 2012). A similar trend was found for HSG-12/DOX and HSG-6/DOX nanoparticles.

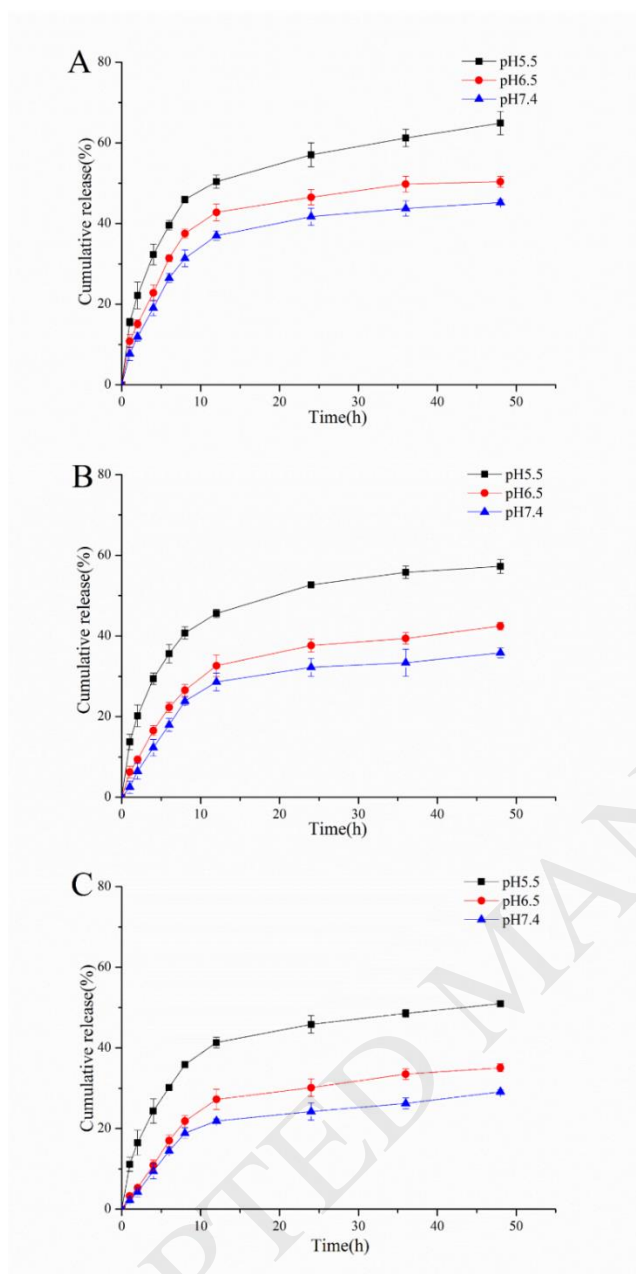


Fig. 3. Release profiles of doxorubicin from HSG nanoparticles under different pH: HSG-6/DOX (A), HSG-12/DOX (B), and HSG-20/DOX (C) (n=3).

The release of DOX from HSG nanoparticles was also dependent on the GA graft ratio. The higher GA graft ratio, the slower the drug release rate. For instance, the fractional release of the HSG-20/DOX, HSG-12/DOX and HSG-6/DOX nanoparticles reached about 29%, 36% and 45% at pH 7.4 after 48 h, respectively. This phenomenon suggests that higher GA content resulted in stronger hydrophobic interaction between the hydrophobic core and drug, which may act as a barrier to

restrict the outward diffusion of DOX from the nanoparticles (Xiangyang et al., 2007).

3.5. *In vitro* cytotoxicity assay

The cytotoxicity of HSG/DOX nanoparticle was investigated in HepG2 cells using an MTT assay. As shown in Fig. 4, free DOX and HSG/DOX nanoparticles exhibited a dose-dependent cytotoxicity to HepG2 cells. And the IC_{50} of DOX solution, HSG-20/DOX, HSG-12/DOX and HSG-6/DOX nanoparticles after 24-h incubation was 0.452, 0.450, 0.518, and 1.169 $\mu\text{g/mL}$, respectively. It was found that only HSG-20/DOX nanoparticles showed cytotoxicity equivalent to that of DOX solution. This result might be explained by the fact that DOX release from the HSG/DOX nanoparticles was incomplete within 24-h incubation period. As evidenced by *in vitro* release profile (Fig. 3), even under acid condition, DOX released from HSG-20/DOX, HSG-12/DOX, and HSG-6/DOX in 24 h were 46%, 53% and 57 %, respectively. Therefore, it is reasonable to deduce that if HSG/DOX nanoparticles are incubated with HepG2 cells for a longer period, they could be more cytotoxic against cancer cells.

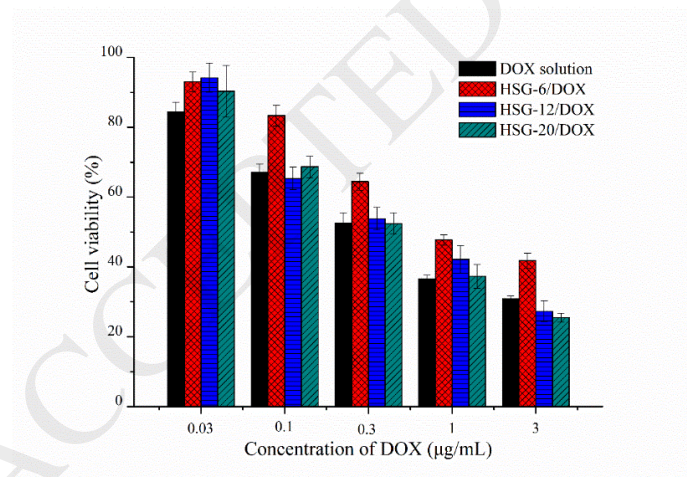


Fig. 4. *In vitro* cytotoxicity of DOX-loaded HSG nanoparticles against HepG2 cells after incubation for 24 h (n=6).

In addition, HSG/DOX nanoparticles exhibited a GA-dependent cytotoxicity to HepG2 cells. When GA ratio was increased from 6% to 12%, the IC_{50} decreased

remarkably, but no statistical difference in cytotoxicity was found at GA ratio 12% and 20%. This could probably be explained by two reasons. First of all, GA ratio can affect the particle size of HSG nanoparticles (Table 1). As reported previously, the smaller size HA micelles facilitated the transport across the cell membrane, therefore increasing the cellular uptake (Liu et al., 2011). Likewise, due to the smaller size of HSG/DOX nanoparticles at higher GA graft ratio, they could be more efficiently taken up by HepG2 cells via an endocytotic process, thus leading to higher cytotoxicity. Secondly, GA can affect the surface properties of nanoparticles. A large number of studies have evidenced that the hydrophobic groups existed both on the surface and inside of the nanoparticles (Park, Lee & Lee, 2005; Zhang, Yao, Zhou, Wang & Zhang, 2013). Chiu et al. confirmed that with the increase of palmitoyl graft ratio, there were more palmitoyl groups exposed on the surface of chitosan nanoparticles (Chiu et al., 2010). Therefore, it is reasonable to assume that some GA molecules also existed on the surface of HSG/DOX nanoparticles, and the larger the GA content, the higher density of GA on the surfaces of the nanoparticles, which could deliver more DOX into HepG2 cells by GA receptor-mediated endocytosis until a saturation was achieved, as observed in the case of GA 12% and 20% samples. This assumption was further demonstrated by the followed pharmacokinetic and tissue distribution studies.

3.6. Pharmacokinetic study in rats

Pharmacokinetics of the HSG/DOX nanoparticles were studied in rats. The plasma concentration-time curves are shown in Fig. 5, and the selected pharmacokinetic parameters are listed in Table 2. As expected, DOX solution showed relatively short halftime and was quickly removed from the plasma. In contrast, the HSG/DOX nanoparticles exhibited a longer and GA-dependent circulation time in plasma. The HSG-20/DOX, HSG-12/DOX, and HSG-6/DOX nanoparticles had significantly higher AUC(0-∞) (22.8, 17.4, and 13.3-fold, respectively), longer $t_{1/2}$ (5.1, 3.7, and 2.4-fold, respectively) and MRT_(0-∞) (9.2, 7.4, and 4.5-fold, respectively), and lower CL (24.6, 18.0, and 14.5-fold, respectively) than that of DOX solution. This

phenomenon might be due to that the hydrophobic inner core of the nanoparticles can serve as a reservoir for DOX to provide sustained release of drug, resulting in prolonged residence of DOX in systemic blood circulation, and this sustained release ability was GA ratio-dependent. This is in good agreement with the *in vitro* release results (Fig. 3). By simulating the bloodstream (pH 7.4) environment, DOX released from HSG-20/DOX, HSG-12/DOX, and HSG-6/DOX in 48 h was 29%, 35% and 45%, respectively. Thus, the nanoparticles with higher GA graft ratio had longer circulation time in plasma. And meanwhile, it is well known that the protein corona formed around nanoparticles upon entering a biological fluid can significantly affect the *in vivo* fate of nanoparticles (Lundqvist, Stigler, Elia, Lynch, Cedervall & Dawson, 2008; Lundqvist. et al., 2011). Contributed to the hydrophilic outer shell and the negative charge, the HSG/DOX nanoparticles were conducive to prevent the unwanted protein adsorption, and thereby avoid the uptake by the reticuloendothelial system (RES) (Choi, Saravanakumar, Park & Park, 2012), leading to reduced clearance rate, thus, GA ratio dependent liver targeting effect was achieved.

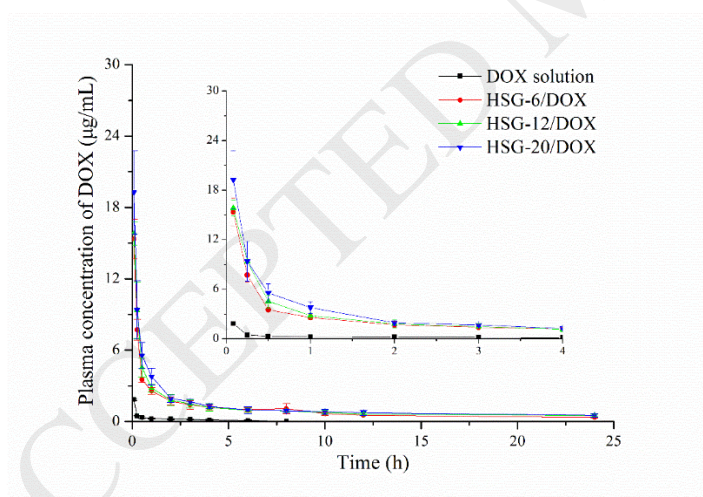


Fig. 5. Mean plasma concentration-time curves after intravenous administration of DOX solution and DOX-loaded HSG nanoparticles at a dose of 5 mg/kg in rats (n=5).

Table 2. Pharmacokinetic parameters after intravenous administration of DOX solution and DOX-loaded HSG nanoparticles in rats at a dose of 5 mg/kg (n=5).

Parameter	DOX solution	HSG-6/DOX	HSG-12/DOX	HSG-20/DOX
AUC(0-∞)(mg/L*h)	2.190±0.916	29.195±4.600	38.208±11.399	49.843±10.062
MRT(0-∞)(h)	2.934±0.900	13.114±1.882	21.701±8.623	27.009±9.210
t _{1/2} (h)	4.640±3.194	11.122±1.991	16.984±8.956	23.570±7.610
CL(L/h/kg)	2.537±0.782	0.175±0.030	0.141±0.041	0.103±0.018
C _{max} (mg/L)	1.840±0.053	15.357±1.663	15.831±0.977	19.615±3.373

Besides, it is well known that particle size can affect the *in vivo* behavior of nanoparticles (Gaumet, Vargas, Gurny & Delie, 2008; Moghimi, Hunter & Murray, 2001), and there are some difference in the particle size of three HSG/DOX nanoparticles (160-260 nm, as shown in Table 1). However, it is reported that carrier systems with diameters of 150-300 nm can be uptaken by RES and then be transported to the liver and spleen (Hickey, Santos, Williford & Mao, 2015). On the other hand, the hydrophilic surface with highly negative charge of the nanoparticles is not conducive to the recognition and phagocytosis of macrophage (Choi, Saravanakumar, Park & Park, 2012), counteracting some of the effect of particle size on the *in vivo* behavior. Therefore, the particle size was not the main reason for the different pharmacokinetic behavior.

3.7. Tissues distribution study

The HSG/DOX nanoparticles were injected intravenously into KM mice to evaluate their tissue distribution. From Fig. 6 and Table 3, it was found that the nanoparticles had superior liver targeting efficiency and the liver targeting capacity was GA ratio dependent. In the liver, the AUC of HSG-20/DOX, HSG-12/DOX, and HSG-6/DOX nanoparticles was 4.0, 3.1 and 2.6-fold higher than that of DOX solution, respectively. As mentioned above, the particle size was not the main reason for the

biodistribution of nanoparticles in the body, because all of these three HSG/DOX nanoparticles (160-260 nm) can induce nonspecific RES uptake of liver (Gaumet, Vargas, Gurny & Delie, 2008) and the hydrophilic surface with highly negative charge could offset partial effect of particle size on hepatic passive targeting. And Tian et al. showed that nanoparticles with similar particle size also presented an increasing liver targeting ability as the GA content increased (Tian, Wang, Wang, Zhang, Liu & Yuan, 2010), which further indicates that the discrepancy of accumulation in the liver is not related to the difference in particle size. Therefore, the GA-dependent liver targeting capacity of the HSG/DOX nanoparticles may be explained as follows: with the increase of GA graft ratio, the density of GA on the surface of the nanoparticles increased, leading to higher binding affinity to the liver region by GA receptor-mediated endocytosis.

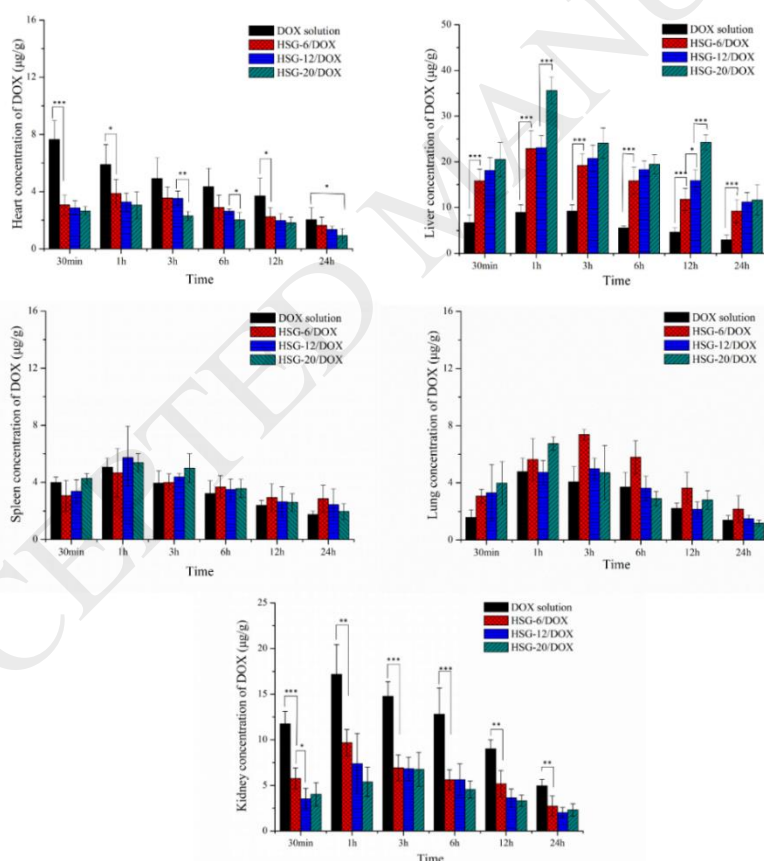


Fig. 6. Tissue distribution of DOX after intravenous administration of DOX solution and DOX-loaded HSG nanoparticles at a dose of 5 mg/kg (n=5). * $p<0.05$. ** $p<0.01$. *** $p<0.001$.

Additionally, the HSG/DOX nanoparticles also could reduce significant amounts of DOX distribution into the heart and kidney. The AUC of HSG-20/DOX, HSG-12/DOX, and HSG-6/DOX nanoparticles was 2.1, 1.7, 1.5-fold, and 2.6, 2.4, 1.9-fold lower than that of DOX solution in the heart and kidney, respectively. It is well known that the major limitation of DOX for successful cancer treatment is primarily ascribed to its indiscriminate distribution in various tissues, thereby result in serious side effects including cardiotoxicity and nephrotoxicity (Tacar, Sriamornsak & Dass, 2013). Therefore, the ability of the HSG/DOX nanoparticles to reduce DOX distribution in the heart and kidney, has important clinical significance for decreasing the side effects of DOX.

Table 3. The AUC after intravenous administration of DOX solution and DOX-loaded HSG nanoparticles in various tissues of mice at a dose of 5 mg/kg (n=5).

Tissue	AUC(0-24) ($\mu\text{g}/\text{g}\cdot\text{h}$)			
	DOX solution	HSG-6/DOX	HSG-12/DOX	HSG-20/DOX
Heart	90.954 \pm 21.251	58.957 \pm 8.713	52.748 \pm 4.242	42.678 \pm 6.332
Liver	123.831 \pm 6.361	322.324 \pm 41.949	387.628 \pm 45.788	497.536 \pm 22.354
Spleen	65.866 \pm 9.990	78.407 \pm 16.464	74.833 \pm 15.396	73.797 \pm 10.856
Lung	62.463 \pm 8.846	90.447 \pm 18.532	65.514 \pm 7.466	78.037 \pm 21.296
Kidney	236.058 \pm 23.632	122.394 \pm 24.371	99.286 \pm 15.855	90.896 \pm 16.277

3.8 Evaluation of tumor targeting effect by *in vivo* imaging

Tissues distribution study only demonstrated the liver-targeting property of HSG/DOX nanoparticles. To evaluate the tumor targeting ability, *in vivo* imaging technique was performed using HepG2 tumor-xenografted mice, and the liver targeting property was further validated.

As shown in Fig. 7A, for the DiR solution group, almost no fluorescence signal in the liver region was observed at 1 h, and the intensity was the strongest at 6 h and then decreased rapidly. Compared with DiR solution, the fluorescence intensity of

HSG/DiR nanoparticles increased significantly at each time point, and reached the highest at 12 h. Moreover, the higher amount of GA content, the stronger the fluorescence signal of HSG/DiR nanoparticles in the liver. The GA-dependent liver targeting ability was further confirmed by the *ex vivo* fluorescent image and semi-quantitative analysis (Fig. 7C and 7B). The accumulation of HSG-20/DiR, HSG-12/DiR, and HSG-6/DiR nanoparticles in the liver was 4.2, 3.2, 2.3-fold higher than that of DiR solution, respectively. This was in good consistent with the results of tissue distribution study.

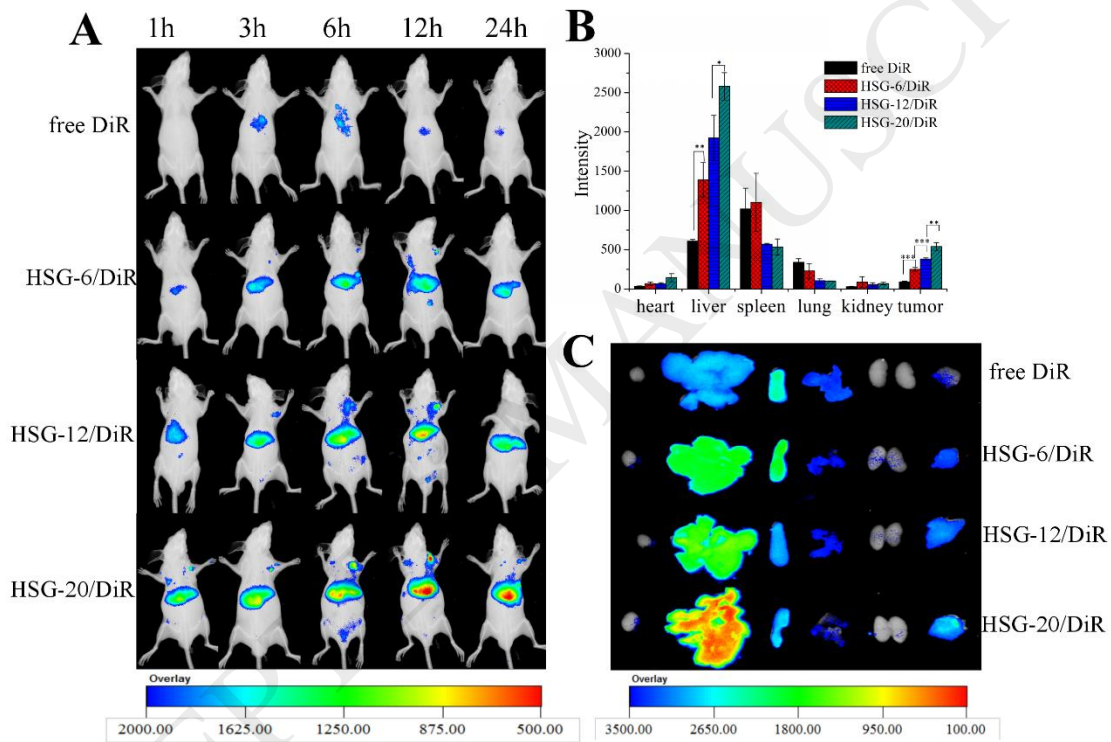


Fig. 7. Fluorescence imaging in KM mice after intravenous administration of free DiR and DiR-loaded HSG nanoparticles, respectively. (A) Time-dependent in vivo images after i.v. injection. (B) *Ex vivo* fluorescence images of tissues at 24 h post-injection. (C) Quantification of the *ex vivo* tissue uptake characteristics after 24 h post-injection (n=3). * $p < 0.05$. ** $p < 0.01$. *** $p < 0.001$.

In the tumor, for the DiR solution group, nothing is visible throughout the detection time. In contrast, the fluorescence intensity of HSG/DiR nanoparticles was significantly stronger, and further strengthened with GA content increase. The

accumulation of HSG-20/DiR, HSG-12/DiR, and HSG-6/DiR nanoparticles in the tumor was 6.0, 4.2, 2.8-fold higher than that of DiR solution, respectively. This could be explained by the fact that HSG nanoparticles can passively target to tumor tissues by the enhanced permeability and retention (EPR) effect and also can actively target the HepG2 solid tumor cells by HA and GA receptor-mediated endocytosis. And the higher GA level of HSG nanoparticles can enhance the GA receptor-mediated endocytosis, thus increasing the accumulation in tumor sites. Simultaneously, smaller particles could penetrate the tumor tissue gaps more easily (Hickey, Santos, Williford & Mao, 2015) and further increase the EPR effect.

In our previous studies(Wang, Gu, Wang, Sun, Wu & Mao, 2017), we found that coupling HA with GA by modifying hydroxyl groups might exhibit higher liver targeting efficiency compared to carboxyl group modification. Encouragingly, in this study, *in vivo* imaging analysis suggested that the nanoparticles synthesized by modifying the hydroxyl groups not only had better liver targeting property, but also presented higher tumor targeting efficiency compared with that of nanoparticles synthesized by modifying carboxyl groups (as shown in Table 4), which further confirmed that the binding site could influence the targeting ability of nanoparticles. Overall, nanoparticles based on HSG conjugates synthesized via modifying hydroxyl groups could be used as promising liver targeting carriers for hydrophobic anti-tumor drugs.

Table 4. Properties comparison of hyaluronic acid-graft-glycyrrhetic acid nanoparticles with different bridging groups.

Sample	Binding site	Bridging group	DS (%)	Liver targeting ability	Tumor targeting ability
HA-Suc-GA (HSG)	Hydroxyl groups	Succinic acid	20.4	4.2-fold higher than that of free DiR at 24 h	6.0-fold higher than that of free DiR at 24 h
HA-Etda-GA (HGA) (Zhang, Yao, Zhou, Wang & Zhang, 2013)	Carboxyl groups	Ethylenediamine	20.2	1.83-fold higher than that of free DiR at 24 h	2.88-fold higher than that of free DiR at 24 h
HA-Cyst-GA (Mezghrani et al., 2015)	Carboxyl groups	Cystamine	23.8	1.8-fold higher than that of free DiR at 24 h	2.6-fold higher than that of free DiR at 24 h

4. Conclusion

In this study, a liver-targeting drug delivery system based on HSG/DOX nanoparticles was prepared for better therapy of hepatocytes. *In vitro* studies showed the HSG/DOX nanoparticles exhibited sustained and pH-dependent DOX release pattern, and GA-dependent cytotoxicity to HepG2 cells. *In vivo* investigation demonstrated that HSG/DOX nanoparticles could prolong blood circulation time, enhance the liver targeting efficiency, and reduce the cardiotoxicity and nephrotoxicity of DOX. Using DiR as a NIR fluorescent dye, the tumor-targeting ability of HSG nanoparticles was further investigated using an *in vivo* imaging technique. The better liver targeting property (4.2-, 3.2-, and 2.3-fold, respectively) and higher tumor targeting efficiency (6.0-, 4.2-, and 2.8-fold, respectively) of HSG-20/DiR, HSG-12/DiR, and HSG-6/DiR nanoparticles were disclosed in comparison with DiR solution. And coupling HA with GA by modifying hydroxyl groups presented higher liver and tumor targeting efficiency compared to carboxyl group modification. In conclusion, HSG conjugates obtained by modifying hydroxyl groups have promising potential as a liver targeting carrier for hydrophobic anti-tumor drugs delivery. Meanwhile, this result also reminds us that not only polymer type, but also the binding site may influence its biological function as a drug carrier, and this point should be taken into consideration in polymer conjugate based nanoparticle design.

Acknowledgments

This project is financially supported by the Natural Science Foundation of China (Grant No. 81273446).

References

- Arpicco, S., Milla, P., Stella, B., & Dosio, F. (2014). Hyaluronic Acid Conjugates as Vectors for the Active Targeting of Drugs, Genes and Nanocomposites in Cancer Treatment. *Molecules*, *19*(3), 3193-3230.
- Bhang, S. H., Won, N., Lee, T.-J., Jin, H., Nam, J., Park, J., Chung, H., Park, H.-S., Sung, Y.-E., Hahn, S. K., Kim, B.-S., & Kim, S. (2009). Hyaluronic Acid-Quantum Dot Conjugates for In Vivo Lymphatic Vessel

Imaging. *Acs Nano* (Vol. 3, pp. 1389-1398).

Cai, Y., Xu, Y., Chan, H. F., Fang, X., He, C., & Chen, M. (2016). Glycyrrhetic Acid Mediated Drug Delivery Carriers for Hepatocellular Carcinoma Therapy. *Molecular Pharmaceutics*, *13*(3), 699-709.

Chiu, Y.-L., Ho, Y.-C., Chen, Y.-M., Peng, S.-F., Ke, C.-J., Chen, K.-J., Mi, F.-L., & Sung, H.-W. (2010). The characteristics, cellular uptake and intracellular trafficking of nanoparticles made of hydrophobically-modified chitosan. *Journal of Controlled Release*, *146*(1), 152-159.

Choi, K. Y., Chung, H., Min, K. H., Yoon, H. Y., Kim, K., Park, J. H., Kwon, I. C., & Jeong, S. Y. (2010). Self-assembled hyaluronic acid nanoparticles for active tumor targeting. *Biomaterials*, *31*(1), 106-114.

Choi, K. Y., Saravanakumar, G., Park, J. H., & Park, K. (2012). Hyaluronic acid-based nanocarriers for intracellular targeting: Interfacial interactions with proteins in cancer. *Colloids and Surfaces B-Biointerfaces*, *99*, 82-94.

Egusquiguirre, S. P., Igartua, M., Hernandez, R. M., & Pedraz, J. L. (2012). Nanoparticle delivery systems for cancer therapy: advances in clinical and preclinical research. *Clin Transl Oncol*, *14*(2), 83-93.

Gaumet, M., Vargas, A., Gurny, R., & Delie, F. (2008). Nanoparticles for drug delivery: The need for precision in reporting particle size parameters. *European Journal of Pharmaceutics and Biopharmaceutics*, *69*(1), 1-9.

Guo, H., Lai, Q., Wang, W., Wu, Y., Zhang, C., Liu, Y., & Yuan, Z. (2013). Functional alginate nanoparticles for efficient intracellular release of doxorubicin and hepatoma carcinoma cell targeting therapy. *International Journal of Pharmaceutics*, *451*(1-2), 1-11.

Guo, H., Zhang, D., Li, T., Li, C., Guo, Y., Liu, G., Hao, L., Shen, J., Qi, L., Liu, X., Luan, J., & Zhang, Q. (2014). In Vitro and In Vivo Study of Gal-OS Self-Assembled Nanoparticles for Liver-Targeting Delivery of Doxorubicin. *Journal of Pharmaceutical Sciences*, *103*(3), 987-993.

Han, S.-Y., Han, H. S., Lee, S. C., Kang, Y. M., Kim, I.-S., & Park, J. H. (2011). Mineralized hyaluronic acid nanoparticles as a robust drug carrier. *Journal of Materials Chemistry*, *21*(22), 7996-8001.

Han, X., Wang, Z., Wang, M., Li, J., Xu, Y., He, R., Guan, H., Yue, Z., & Gong, M. (2016). Liver-targeting self-assembled hyaluronic acid-glycyrrhetic acid micelles enhance hepato-protective effect of silybin after oral administration. *Drug Delivery*, *23*(5), 1818-1829.

Hickey, J. W., Santos, J. L., Williford, J.-M., & Mao, H.-Q. (2015). Control of polymeric nanoparticle size to improve therapeutic delivery. *Journal of Controlled Release*, *219*, 536-547.

Hokputsa, S., Jumel, K., Alexander, C., & Harding, S. E. (2003). Hydrodynamic characterisation of chemically degraded hyaluronic acid. *Carbohydrate Polymers*, *52*(2), 111-117.

Huo, M., Zou, A., Yao, C., Zhang, Y., Zhou, J., Wang, J., Zhu, Q., Li, J., & Zhang, Q. (2012). Somatostatin receptor-mediated tumor-targeting drug delivery using octreotide-PEG-deoxycholic acid conjugate-modified N-deoxycholic acid-O, N-hydroxyethylation chitosan micelles. *Biomaterials*, *33*(27), 6393-6407.

Jiang, H.-L., Kim, Y.-K., Arote, R., Jere, D., Quan, J.-S., Yu, J.-H., Choi, Y.-J., Nah, J.-W., Cho, M.-H., & Cho, C.-S. (2009). Mannosylated chitosan-graft-polyethylenimine as a gene carrier for Raw 264.7 cell targeting. *International Journal of Pharmaceutics*, *375*(1-2), 133-139.

Kataoka, K., Matsumoto, T., Yokoyama, M., Okano, T., Sakurai, Y., Fukushima, S., Okamoto, K., & Kwon, G. S. (2000). Doxorubicin-loaded poly(ethylene glycol)-poly(b-benzyl-L-aspartate) copolymer micelles: their pharmaceutical characteristics and biological significance. *Journal of Controlled Release*, *98*, 143-153.

Krishna, A. D. S., Mandraju, R. K., Kishore, G., & Kondapi, A. K. (2009). An Efficient Targeted Drug

Delivery through Apotransferrin Loaded Nanoparticles. *Plos One*, 4(10).

Lao, S.-B., Zhang, Z.-X., Xu, H.-H., & Jiang, G.-B. (2010). Novel amphiphilic chitosan derivatives: Synthesis, characterization and micellar solubilization of rotenone. *Carbohydrate Polymers*, 82(4), 1136-1142.

Li, C., & Wallace, S. (2008). Polymer-drug conjugates: Recent development in clinical oncology. *Advanced Drug Delivery Reviews*, 60(8), 886-898.

Liu, Y. H., Sun, J., Cao, W., Yang, J. H., Lian, H., Li, X., Sun, Y. H., Wang, Y. J., Wang, S. L., & He, Z. G. (2011). Dual targeting folate-conjugated hyaluronic acid polymeric micelles for paclitaxel delivery. *International Journal of Pharmaceutics*, 421(1), 160-169.

Lu, Y., Li, J., & Wang, G. (2008). In vitro and in vivo evaluation of mPEG-PLA modified liposomes loaded glycyrrhetic acid. *International Journal of Pharmaceutics*, 356(1-2), 274-281.

Lundqvist, M., Stigler, J., Elia, G., Lynch, I., Cedervall, T., & Dawson, K. A. (2008). Nanoparticle size and surface properties determine the protein corona with possible implications for biological impacts. *Proc Natl Acad Sci U S A*, 105(38), 14265-14270.

Lundqvist, M., Stigler, J., Cedervall, T., Berggard, T., Flanagan, M. B., Lynch, I., Elia, G., & Dawson, K. (2011). The Evolution of the Protein Corona around Nanoparticles: A Test Study. *Acs Nano*, 5, 7503-7509.

Matsumura, Y., & Kataoka, K. (2009). Preclinical and clinical studies of anticancer agent-incorporating polymer micelles. *Cancer Science*, 100(4), 572-579.

Mezghrani, O., Tang, Y., Ke, X., Chen, Y., Hu, D., Tu, J., Zhao, L., & Bourkaib, N. (2015). Hepatocellular carcinoma dually-targeted nanoparticles for reduction triggered intracellular delivery of doxorubicin. *International Journal of Pharmaceutics*, 478(2), 553-568.

Moghimi, S. M., Hunter, A. C., & Murray, J. C. (2001). Long-circulating and target-specific nanoparticles: theory to practice. *Pharmacological reviews*, 53(2), 283-318.

Park, E. K., Lee, S. B., & Lee, Y. M. (2005). Preparation and characterization of methoxy poly(ethylene glycol)/poly(epsilon-caprolactone) amphiphilic block copolymeric nanospheres for tumor-specific folate-mediated targeting of anticancer drugs. *Biomaterials*, 26(9), 1053-1061.

Schante, C. E., Zuber, G., Herlin, C., & Vandamme, T. F. (2011). Chemical modifications of hyaluronic acid for the synthesis of derivatives for a broad range of biomedical applications. *Carbohydrate Polymers*, 85(3), 469-489.

Schiffelers, R. M., Ansari, A., Xu, J., Zhou, Q., Tang, Q. Q., Storm, G., Molema, G., Lu, P. Y., Scaria, P. V., & Woodle, M. C. (2004). Cancer siRNA therapy by tumor selective delivery with ligand-targeted sterically stabilized nanoparticle. *Nucleic Acids Research*, 32(19).

Shuai, X., Ai, H., Nasongkla, N., Kim, S., & Gao, J. (2004). Micellar carriers based on block copolymers of poly(epsilon-caprolactone) and poly(ethylene glycol) for doxorubicin delivery. *Journal of Controlled Release*, 98(3), 415-426.

Son, G. M., Kim, H. Y., Ryu, J. H., Chu, C. W., Kang, D. H., Park, S. B., & Jeong, Y.-I. (2014). Self-Assembled Polymeric Micelles Based on Hyaluronic Acid-g-Poly(D,L-lactide-co-glycolide) Copolymer for Tumor Targeting. *International Journal of Molecular Sciences*, 15(9), 16057-16068.

Tacar, O., Sriamornsak, P., & Dass, C. R. (2013). Doxorubicin: an update on anticancer molecular action, toxicity and novel drug delivery systems. *Journal of Pharmacy and Pharmacology*, 65(2), 157-170.

Tian, Q., Wang, X., Wang, W., Zhang, C., Liu, Y., & Yuan, Z. (2010). Insight into glycyrrhetic acid: The role of the hydroxyl group on liver targeting. *International Journal of Pharmaceutics*, 400(1-2), 153-157.

- Tian, Q., Wang, X. H., Wang, W., Zhang, C. N., Wang, P., & Yuan, Z. (2012). Self-assembly and liver targeting of sulfated chitosan nanoparticles functionalized with glycyrrhetic acid. *Nanomedicine*, 8(6), 870-879.
- Tian, Q., Zhang, C.-N., Wang, X.-H., Wang, W., Huang, W., Cha, R.-T., Wang, C.-H., Yuan, Z., Liu, M., Wan, H.-Y., & Tang, H. (2010). Glycyrrhetic acid-modified chitosan/poly(ethylene glycol) nanoparticles for liver-targeted delivery. *Biomaterials*, 31(17), 4748-4756.
- Torre, L. A., Bray, F., Siegel, R. L., Ferlay, J., Lortet-Tieulent, J., & Jemal, A. (2015). Global Cancer Statistics, 2012. *Ca-a Cancer Journal for Clinicians*, 65(2), 87-108.
- Tripodo, G., Trapani, A., Torre, M. L., Giammona, G., Trapani, G., & Mandracchia, D. (2015). Hyaluronic acid and its derivatives in drug delivery and imaging: Recent advances and challenges. *European Journal of Pharmaceutics and Biopharmaceutics*, 97, 400-416.
- Wang, L. L., Sun, Y. J., Shi, C. J., Li, L., Guan, J., Zhang, X., Ni, R., Duan, X. P., Li, Y. P., & Mao, S. R. (2014). Uptake, transport and peroral absorption of fatty glyceride grafted chitosan copolymer-enoxaparin nanocomplexes: Influence of glyceride chain length. *Acta Biomaterialia*, 10(8), 3675-3685.
- Wang, X., Gu, X., Wang, H., Sun, Y., Wu, H., & Mao, S. (2017). Synthesis, characterization and liver targeting evaluation of self-assembled hyaluronic acid nanoparticles functionalized with glycyrrhetic acid. *European Journal of Pharmaceutical Sciences*, 96, 255-262.
- Wang, X. H., Tian, Q., Wang, W., Zhang, C. N., Wang, P., & Yuan, Z. (2012). In vitro evaluation of polymeric micelles based on hydrophobically-modified sulfated chitosan as a carrier of doxorubicin. *Journal of materials science. Materials in medicine*, 23(7), 1663-1674.
- Wu, J.-l., Liu, C.-g., Wang, X.-l., & Huang, Z.-h. (2012). Preparation and characterization of nanoparticles based on histidine-hyaluronic acid conjugates as doxorubicin carriers. *Journal of Materials Science-Materials in Medicine*, 23(8), 1921-1929.
- Xiangyang, X., Ling, L., Jianping, Z., Shiyue, L., Jie, Y., Xiaojin, Y., & Jinsheng, R. (2007). Preparation and characterization of N-succinyl-N'-octyl chitosan micelles as doxorubicin carriers for effective anti-tumor activity. *Colloids and surfaces. B, Biointerfaces*, 55(2), 222-228.
- Zhang, C., Wang, W., Liu, T., Wu, Y., Guo, H., Wang, P., Tian, Q., Wang, Y., & Yuan, Z. (2012). Doxorubicin-loaded glycyrrhetic acid-modified alginate nanoparticles for liver tumor chemotherapy. *Biomaterials*, 33(7), 2187-2196.
- Zhang, L., Yao, J., Zhou, J., Wang, T., & Zhang, Q. (2013). Glycyrrhetic acid-graft-hyaluronic acid conjugate as a carrier for synergistic targeted delivery of antitumor drugs. *International Journal of Pharmaceutics*, 441(1-2), 654-664.

Figure legends

Fig. 1. Particle size distribution measured by dynamic light scattering (DLS) (A) and TEM image (B) of the HSG-12/DOX nanoparticles prepared at drug-to-carrier ratio of 20%.

Fig. 2. DSC spectra of DOX, HSG-12 blank nanoparticles, physical mixture of DOX and blank HSG nanoparticles, and HSG-12/DOX nanoparticles.

Fig. 3. Release profiles of doxorubicin from HSG nanoparticles under different pH: HSG-6/DOX (A), HSG-12/DOX (B), and HSG-20/DOX (C) (n=3).

Fig. 4. In vitro cytotoxicity of DOX-loaded HSG nanoparticles against HepG2 cells after incubation for 24 h (n=6).

Fig. 5. Mean plasma concentration-time curves after intravenous administration of DOX solution and DOX-loaded HSG nanoparticles at a dose of 5 mg/kg in rats (n=5).

Fig. 6. Tissue distribution of DOX after intravenous administration of DOX solution and DOX-loaded HSG nanoparticles at a dose of 5 mg/kg (n=5). * $p < 0.05$. ** $p < 0.01$. *** $p < 0.001$.

Fig. 7. Fluorescence imaging in KM mice after intravenous administration of free DiR and DiR-loaded HSG nanoparticles, respectively. (A) Time-dependent in vivo images after i.v. injection. (B) Ex vivo fluorescence images of tissues at 24 h post-injection. (C) Quantification of the ex vivo tissue uptake characteristics after 24 h post-injection (n=3). * $p < 0.05$. ** $p < 0.01$. *** $p < 0.001$.